International Journal of Computer Information Systems and Industrial Management Applications
ISSN 2150-7988 Volume 18(15s) 2026 pp. 968-981
https://doi.org/10.70917/ijcisim-2026-4495
Article

Regional Modeling of Atmospheric Attenuation for Ku- and Ka-Band Satellite Links over Iraq

Taghreed A. Noori[1], Hasanain A. H. Al-Behadili[2]

[1,2]Department of Electrical Engineering, College of Engineering, University of Misan, Maysan, Iraq
Corresponding author E-mail: enghs2306@uomisan.edu.iq

Abstract: A satellite propagation model has been developed for Ku- and Ka-band propagation over three regions in Iraq: Erbil, Baghdad and Amarah, and this propagation model is presented in this paper. The model is a generalized GEO reference link with region-specific environmental inputs from NASA POWER and MERRA-2 aerosol reanalysis from January 2023 to December 2025. The free space loss is determined according to ITU-R P.525, the rain attenuation is determined according to ITU-R P.838 with clearly defined wettest-day mean-intensity proxy and the gaseous attenuation is determined according to ITU-R P.676-13, using pressure, temperature and water-vapour density. The dust attenuation is obtained from a Rayleigh extinction formula, published dielectric properties, and the five-official dust-bin radii and densities in MERRA-2. The monthly bulk DUSMASS product does not include mass fractions per bin, so the highest mass-extinction coefficient for the month in the five bins is selected as the conservative upper limit. Across the four operating cases, mean atmospheric attenuation ranges from 0.095 to 0.101 dB at 12 GHz, 0.122 to 0.131 dB at 14 GHz, 0.418 to 0.456 dB at 20 GHz, and 0.491 to 0.544 dB at 30 GHz. Most of the mean loss is due to gaseous absorption, the second source of loss is rain and direct dust attenuation is less than 4.8×10^{-4} dB for the present monthly concentration and path assumptions. The received power for Mean (30-GHz) is around -84.1dBm for all three cities and the percentages vary quickly when the reference level is close to the received-power range during the month. The study demonstrates that the regional aerosol loading can be simulated in the satellite-link without directly considering the optical or surface mass variables as microwave loss. This results in a framework which is transparent, repeatable and can be used for comparative planning studies and the limitations are clearly defined, allowing distinction between simulated link behaviour and measured operational availability.
Keywords: satellite propagation, Ku-band, Ka-band, Iraq, NASA POWER, MERRA-2, gaseous attenuation, dust attenuation, link budget, reliability indicator.

1. Introduction

Satellite communication remains vital in those areas where terrestrial communication is not possible or is impractical. Earth-space radio paths play a vital role in broadcasting, broadband access, emergency co-ordination, remote teaching, maritime communications, aeronautical communications, and numerous government services. The link budget dominates over these systems, which are very long-distance. When the available fade margin is small or very high Ku- and Ka-band frequencies are utilized, the effects of the atmosphere are more significant and result in smaller absolute fade margin [1]-[5].

Not all the frequencies are affected by the atmosphere equally. Absorption and scattering caused by rain is typically a function of frequency and rain rate. Spectrally structured gaseous loss comes from the presence of molecular oxygen and water vapour. The absorption and scattering of electromagnetic energy can also occur if the particles are suspended, but this depends on the particle size, dielectric properties, concentration, humidity and the geometry of the path [12]-[16]. Therefore, a regional propagation study must account for the difference between the observations of the environment and the physical equations that are used to transform those observations into link attenuation.

The context for this problem is Iraq. The nation runs from the cooler and higher elevation northern region, to the alluvial plain in the middle, to the hotter southern region. In addition to dust activity, the national precipitation, humidity, temperature and pressure are also not uniform throughout the country or throughout the seasons [16]-[19]. The differences are significant enough to warrant a common simulation model with a set of satellite-link assumptions that can be used for various regional environmental inputs. This type of design will enable the effects of location and frequency to be studied separately from any differences in type of terminal.

The NASA POWER meteorological data and the NASA MERRA-2 aerosol reanalysis are used in the study. POWER offers uniform time series of corrected precipitation, near surface temperature, relative humidity and surface pressure [6]. The monthly aerosol diagnostics, such as dust surface mass concentration, are available in MERRA-2 and are frequently employed in applications where a long consistent aerosol record is needed [7]-[10], [24]. These data are used to characterize the environment at the regional level. They are not alone capable of giving the microwave attenuation value. Specifically, if a particle-model and path-model are not available, optical depth and surface mass concentration cannot be directly added to a Ku- or Ka-band link budget.

The present work is a simulation study and not a field measurement campaign. Satellite beacon data, particle size observations, vertical dust profiles and operating-system logs were not available at all the three sites throughout the entire study period. A generic GEO reference link is thus used for the calculation of the received power for a set of common assumptions. The model is for comparative analysis and methodological transparency. It does not state the availability of a particular satellite service.

The paper adds a single and repeatable workflow in four ways. It analyzes 36 environmental samples per month for Erbil, Baghdad and Amarah for 3 years (2023-2025). Secondly, it uses the free space attenuation calculated by ITU-R procedures, in addition to those of rain and gaseous attenuation. Third, it correlates MERRA-2 DUSMASS to microwave extinction using a Rayleigh model that utilizes published microwave dielectric properties and official dust-bin properties, but assumes conservatively unknown bin fractions. Fourth, it relates some of the atmospheric terms to a reference link budget and explores threshold and concentration sensitivity. From this model, the resulting model can be used as a documented basis for discussing differences in propagation over Iraqi areas without introducing unverified conversion factors.

2. Related Work and Research Gap

Weather-related component that has the most development is rain attenuation. The frequency- and polarization-dependent power law for specific attenuation (SPA) is given by ITU-R P.838 and the rain statistics and Earth-space geometry for availability prediction are given in ITU-R P.618 [2, 4]. Ka-band links are very susceptible to heavy rain as shown in the measurement study conducted in South Korea, and the need for regional input data is evident from the modelling study performed in Nigeria [20, 21]. It is also demonstrated here that the time resolution of the rain input is extremely important in these studies.

The attenuation of gasses is a result of molecular absorption and not a single smooth frequency trend. The spectral line parameters and the atmospheric state are used to calculate the attenuation of oxygen and water-vapour by the ITU-R P.676 [5]. Similarly, the line widths and strengths are affected by pressure, temperature and water-vapour density, making use of only the frequency for the atmospheric calculation not a good representation of the monthly regional variation. The direct P.676 procedure is somewhat more complex but is traceable and can be adapted to the physical variables that are available in NASA POWER.

There are a number of methods for conducting dust propagation studies such as Rayleigh or Mie scattering, visibility based relations, particle size measurement, and empirical regressions [12]–[16]. Mie and Rayleigh treatments were described by Sharif [12] with the help of the frequency dependent dielectric properties. Musa et al. [13] and [14] found that the reported attenuation is quite variable as a function of the assumed particle population and storm severity. The importance of specifying the shape, size, concentration and dielectric behavior of the particles in order to interpret a dust-loss estimate was also reiterated by Alozie et al. [15].

There is a strong environmental motivation in the observations made by the Iraqis. Abdulla et al., [16] measured particle-size distributions of sand and dust storms in Iraq and discussed their applications to microwave systems. Subsequent climate studies have been conducted to record the changes in dust event frequency, source and transport [17]-[19]. These publications do not represent a general conversion from an Iraqi surface concentration for a monthly re-analysis to the slant-path satellite attenuation but they do support the use of dust in an Iraqi propagation study.

The other area of the gap is between the regional data and the link modelling. Most simulations are described in detail, but less detail is provided for the meteorological data used, the vertical meaning, and the assumptions on aerosols in the conversion from aerosol to attenuation. This paper attempts to fill that gap by making the environmental inputs, propagation equations, linking assumptions and the treatment of uncertainty separate and explicit. The goal is not to demonstrate that the dust will never be the dominating factor, or always be the negligible factor. It is to make calculations of the direct attenuation using the data provided, and to determine the conditions under which this conclusion would not hold true.

3. Data and Methods

3.1 Study sites and data sources

The three cities of Erbil, Baghdad and Amarah were chosen as representative of the north, central and south of the country. The sites do not constitute a full classification of Iraqi climate zones, but rather a site that was deemed useful for a geographic transect. A common reference link was used for all three sites to reduce the influence of differences in output due to differences in terminal configuration, to the effect that differences in output are caused by differences in environmental input.

Table 1. Study sites used in the regional simulation.

City	Latitude	Longitude	Regional representation
Erbil	36.19° N	44.01° E	Northern Iraq
Baghdad	33.31° N	44.36° E	Central Iraq
Amarah	31.85° N	47.15° E	Southern Iraq

The daily NASA POWER records were used for a period from 1 January 2023 to 31 December 2025. The variables chosen for the processing were corrected precipitation (PRECTOTCORR), 2-m relative humidity (RH2M), 2-m air temperature (T2M) and surface pressure (PS). The MERRA-2 M2TMNXAER aerosol-diagnostics product was used from NASA Giovanni to provide monthly dust surface mass concentration. M2TMNXAER is a product made on a monthly mean basis and contains the DUSMASS field that was utilized for this analysis [6]-[10].

3.2 Quality control and monthly preprocessing

The POWER files were examined for missing columns, duplicate dates, and missing value marker (-999). Each site contained 1,096 daily records covering the full period from 1-January 2023 to 31-December 2025, and no missing markers were found in the selected variables. Daily data was aggregated by month of the calendar year. Averaging of temperature, relative humidity, and pressure. The amount of the wettest day of each month was divided by 24 h to create a wettest-day mean rain intensity:

$$R_m = \max(P_{daily,m}) / 24 \qquad (1)$$

This variable is a monthly comparison input. It is not a "one-minute" rain rate, nor is it the ITU-R R0.01 statistic. It is maintained as a distinction as the POWER record is on a daily basis. The water-vapour density was determined from temperature and relative humidity using the Bolton saturation-vapour-pressure formula [22]:

$$e_s = 6.112 \exp\left[17.67\, T_c / (T_c + 243.5)\right] \qquad (2)$$

$$e = (RH/100)\, es,\ \rho_v = 216.7\, e / T_k \qquad (3)$$

T_c here represents the temperature in degrees Celsius (C), T_k is the absolute temperature, e and e_s are in hectopascals (hPa) and ρ_v is water-vapour density, in grams per cubic meter (g/m³). The records of dust and meteorology for each month were then combined by date, giving 36 complete records for each city.

3.3 Reference satellite-link scenario

A generalized GEO link was used as a fixed simulation environment. The same transmit power, antenna gains, path length and elevation angle were used for all cities. The 12- and 20-GHz cases were labelled downlinks, while 14 and 30 GHz were labelled uplinks to represent common Ku/Ka operating pairs. These values are study assumptions and are not an indication of a named satellite operator/terminal.

Table 2. Reference link and path assumptions.

Parameter	Value	Purpose
Transmit power, P_t	40 dBm	Fixed reference value
Transmit antenna gain, G_t	45 dBi	Fixed reference value
Receive antenna gain, G_r	45 dBi	Fixed reference value
Slant distance, d	38,000 km	Generalized GEO path
Elevation angle, θ	45°	Common comparison angle
Rain-layer height	2 km	Comparative rain path
Dust-layer height	3 km	Uniform sensitivity layer
Frequencies	12, 14, 20, 30 GHz	Ku/Ka cases

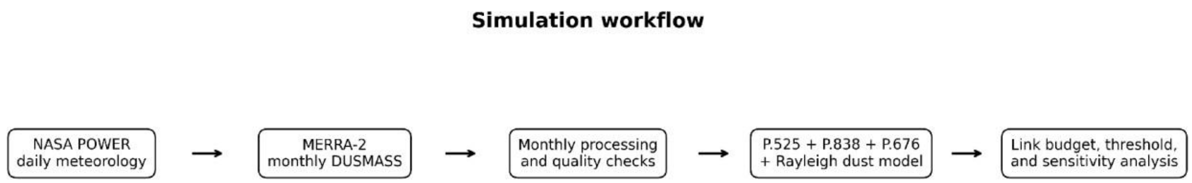

Fig. 1. Data processing and propagation-simulation workflow.

3.4 Free-space and rain attenuation

The free space path loss was estimated from ITU-R P.525 with frequency in gigahertz and distance in kilometers [3]:

$$\mathrm{FSPL} = 92.45 + 20\log_{10}(f_{GHz}) + 20\log_{10}(d_{km}) \quad (4)$$

The power law for the attenuation as a function of polarization was the same for rain as for ITU-R P.838 (horizontal polarization):

$$\gamma R = kR_{m}{}^{\wedge}\alpha \quad (5)$$

$$A_{rain} = \gamma R_{hr} / \sin\theta \quad (6)$$

The coefficients k and α were evaluated at 12, 14, 20, and 30 GHz. Because R_m is a wettest-day mean intensity, A_{rain} is interpreted as a consistent monthly propagation indicator rather than an annual exceedance statistic. A service-availability study would require one-minute or validated hourly rain statistics and the full ITU-R P.618/P.837 procedure [2], [23].

3.5 Gaseous attenuation

The oxygen and water-vapour attenuation was determined using the line tables from the ITU-R P.676-13 [5]. The line equations were fed with monthly pressure, temperature and water-vapour density. The equivalent oxygen and water-vapour heights were used in Annex 2: Method 1 (slant-path loss).

$$A_{gas} = (\gamma_o h_o + \gamma_w h_w) / \sin\theta \quad (7)$$

The calculation is done for 44 oxygen lines and 35 water-vapour lines. The "oxy" and "water-vap" terms were kept separate and added together. This method allows the water-vapour influence on the absorption spectrum to be preserved, especially the high-frequency and high-intensity portion at 20 GHz.

3.6 Dust extinction model

MERRA-2 is the five dry mass bins of dust. Their nominal radii are 0.73, 1.4, 2.4, 4.5, and 8.0 µm. The density is 2,500 kg/m³ for DU001 and 2,650 kg/m³ for DU002-DU005 [11]. In the GEOS aerosol scheme, the particles are assumed to be hydrophobic. It was found that the complex dielectric constant had to be adjusted according to the reported relation on humidity, and the particle radius was kept dry.

The Rayleigh extinction cross section was calculated for a spherical particle of radius a, wavenumber k_0, and complex relative permittivity $\varepsilon = \varepsilon' + j\varepsilon''$, and was determined to be equal to the sum of the scattering cross section and the absorption cross section:

$$\sigma_{ext} = (8/3)\ \pi a^2 (k_0 a)^4\ |(\varepsilon-1)/(\varepsilon+2)|^2 + 12\pi a^2 (k_0 a)\ \varepsilon'' / [(\varepsilon'+2)^2 + \varepsilon''^2] \quad (8)$$

$$\kappa = \sigma_{ext} / [(4/3)\ \pi a^3 \rho\_p] \quad (9)$$

$$A_{dust} = 4.343\ \kappa\ C_d\ (1000)\ L_d \quad (10)$$

In this case, κ is the mass- extinction coefficient (m²/kg), C_d is DUSMASS (kg/m³), and L_d is the slant path through the 3 km thick dust layer. The number 1000 is used to change from kilometres to metres. All frequencies and bins were checked for the Rayleigh size parameter $k_0 a$, which was largest at 0.00503 for 30 GHz.

The monthly bulk DUSMASS product does not include mass fraction values for each of the 5 bins. Therefore, the model assesses all bins and takes the maximum of the value of κ as the safe upper bound. Additionally, minimum and mean-bin results were kept for uncertainty analysis. This method doesn't create bins that do not exist in the downloaded data.

3.7 Uncertainty and sensitivity treatment

The interpretation was under controlled by using three checks. Firstly, the Rayleigh validity parameter was investigated instead of being assumed. Second, the range of κ between the five MERRA-2 bins was reported at each frequency. Third, the peak DUSMASS was multiplied by four orders of magnitude to find what increase in concentration is needed to get 0.01, 0.1 and 1 dB of dust attenuation at 30 GHz. These tests are not meant to replace field validation tests but are used to show that the conclusion was not adversely affected by the unresolved particle mixture or by concentration scaling.

3.8 Received power and threshold indicator

$$A_{total} = A_{rain} + A_{gas} + A_{dust} \quad (11)$$

$$P_r = P_t + G_t + G_r - FSPL - A_{total} \quad (12)$$

The monthly link indicator was computed for a certain received-power threshold (T):

$$I_T = (100/N)\ \Sigma\ 1[P_{r,m} \geq T] \quad (13)$$

N is the number of months and 1[·] is the indicator function. IT is only used as a comparison to cities and thresholds under the reference link. It is not a rate of reliability of a measured receiver or an annual operational availability rate.

4. Results

4.1 Environmental inputs

Any meteorological conditions were different at the three sites, but similar in each. The mean wettest-day rain input was the greatest for Erbil and the mean temperature was the greatest for Amarah. The water-vapour densities in the cities were similar on a monthly basis because of the counteracting effect of relative humidity and temperature. The highest regional variability was found in DUSMASS where the mean concentrations in the city of Baghdad and Amarah were about 3 and 3.6 times of Erbil, respectively.

Table 3. Summary of the monthly environmental inputs, 2023-2025.

City	Mean Rm	Max Rm	RH (%)	T (°C)	ρv (g/m³)	Mean DUSMASS	Peak DUSMASS

Erbil	0.349	1.465	40.7	22.1	7.11	9.00e-08	1.68e-07
Baghda d	0.326	1.478	37.1	24.8	7.56	2.70e-07	4.89e-07
Amarah	0.271	1.433	32.3	26.8	6.99	3.23e-07	5.91e-07

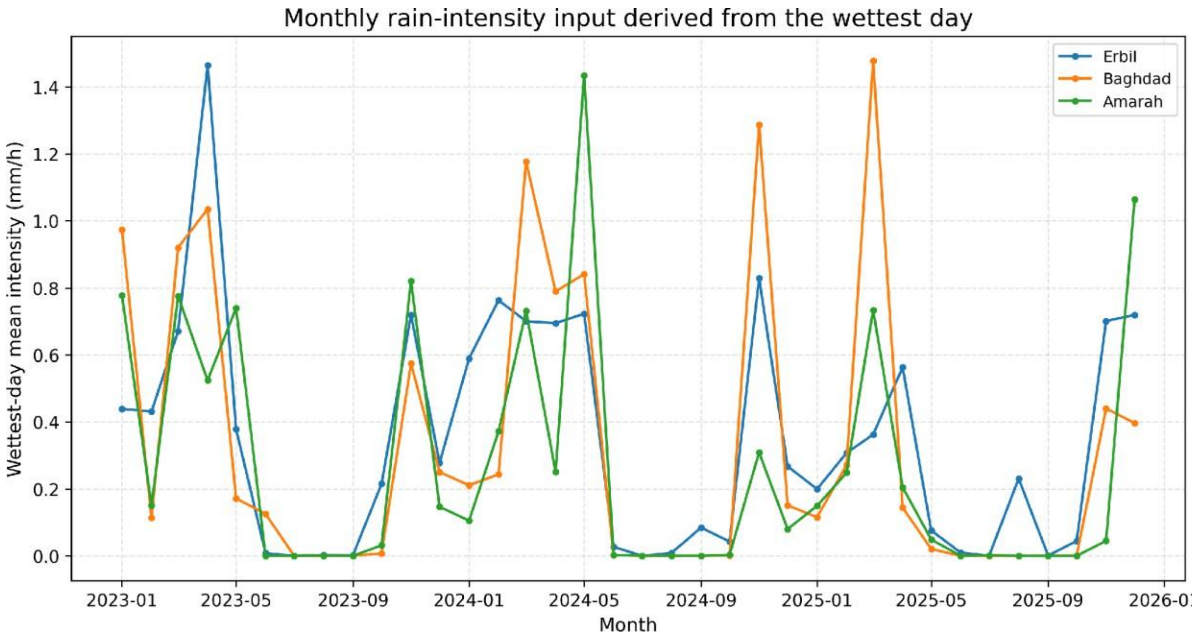

Fig. 2. Monthly rain-intensity input derived from the wettest daily precipitation total.

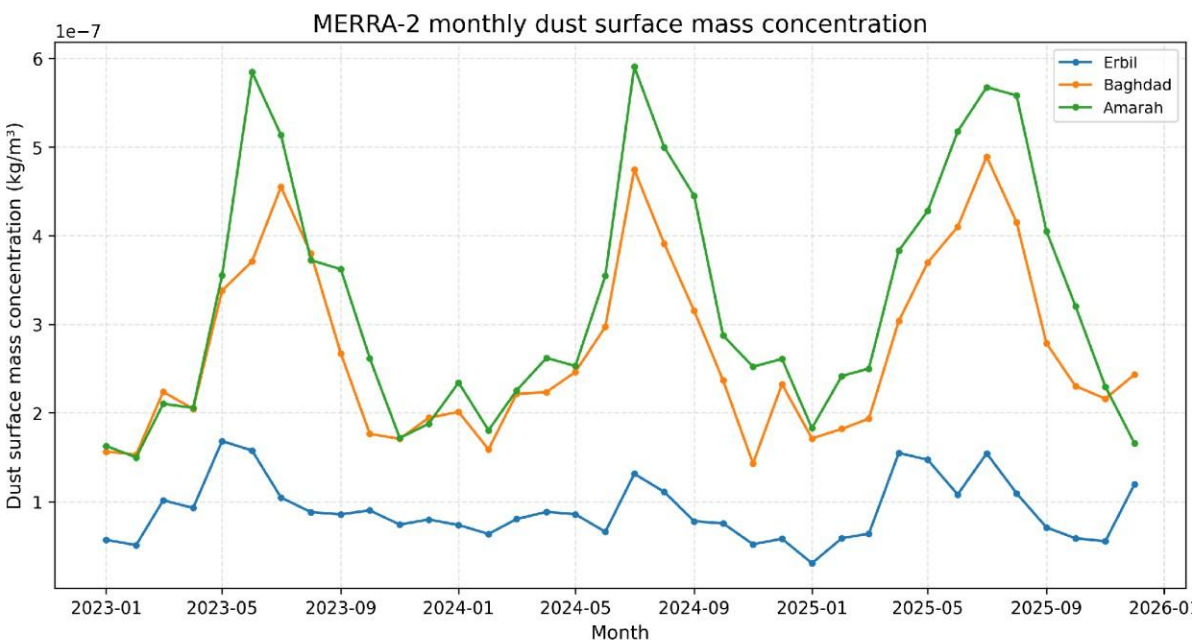

Fig. 3. MERRA-2 monthly dust surface mass concentration over the three study sites.

The dust records showed a regular warm season trend, especially in Baghdad and Amarah. Peak concentrations reached 1.68×10^{-7} kg/m³ in Erbil, 4.89×10^{-7} kg/m³ in Baghdad, and 5.91×10^{-7} kg/m³ in Amarah. These values are for monthly mean surface loading and do not represent storm concentrations in the in-plume.

4.2 Gaseous attenuation

The gaseous attenuation has been found to be around 0.08 dB at 12 GHz, 0.35-0.37 dB at 20 GHz and 0.30-0.32 dB at 30 GHz. The non-monotonic behaviour is followed by the contribution of the water vapour near 20 GHz. The monthly pressure and water-vapour density range for the cities were not very different from each other as there was an overlap in the ranges.

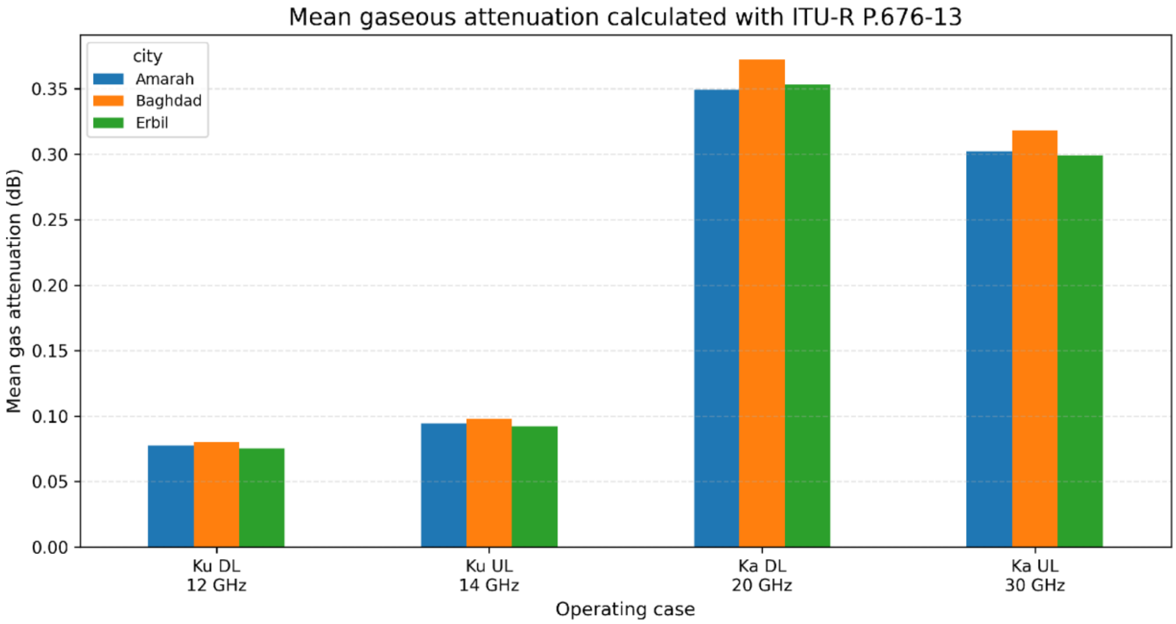

Fig. 4. Mean gaseous attenuation from ITU-R P.676-13.

4.3 Dust mass-extinction coefficient

The mass extinction coefficient was found to be rising with frequency, with a fairly limited range in the five MERRA-2 bins. The maximum coefficient was 0.0224 m²/kg at 12 GHz and 0.0822 m²/kg at 30 GHz. The maximum Rayleigh parameter was found to be less than 0.006, thus, the small particle approximation is valid for the chosen bin radii and frequencies.

Table 4. Dust mass-extinction coefficient across the five MERRA-2 bins.

Frequency (GHz)	κ min (m²/kg)	κ mean (m²/kg)	κ max (m²/kg)	max k_0a
12	0.01979	0.02064	0.02238	0.002012
14	0.02308	0.02408	0.02611	0.002347
20	0.03873	0.03997	0.04296	0.003353
30	0.07534	0.07702	0.08223	0.005030

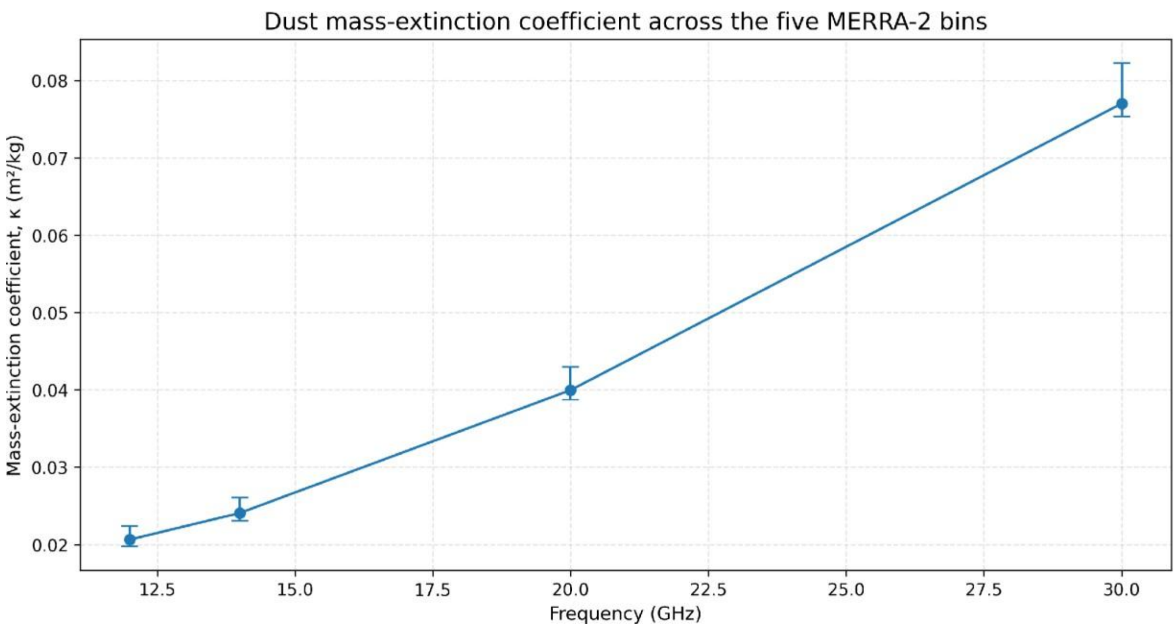

Fig. 5. Frequency-dependent range of the dust mass-extinction coefficient across the five MERRA-2 bins.

4.4 Atmospheric attenuation and received power

Table 5 presents the results of the simulations. The mean total attenuation of the atmosphere was approximately 0.1 dB for the Ku downlink, 0.12-0.13 dB for the Ku uplink, 0.42-0.46 dB for the Ka downlink and 0.49-0.54 dB for the Ka uplink. The regional ordering was not identical at every frequency because the rain and gas terms varied differently from dust concentration.

Table 5. Mean attenuation components and predicted received power.

City	Case	Rain	Gas	Dust	Total	Mean Pr	Min Pr
Erbil	Ku DL (12)	0.0215	0.0755	0.000036	0.0970	-75.726	-75.817
Erbil	Ku UL (14)	0.0344	0.0923	0.000042	0.1267	-77.095	-77.234
Erbil	Ka DL (20)	0.0877	0.3532	0.000070	0.4410	-80.507	-80.871
Erbil	Ka UL (30)	0.2435	0.2990	0.000134	0.5427	-84.131	-84.909
Baghdad	Ku DL (12)	0.0210	0.0799	0.000107	0.1010	-75.730	-75.821
Baghdad	Ku UL (14)	0.0332	0.0979	0.000125	0.1312	-77.099	-77.237

Baghdad	Ka DL (20)	0.0831	0.3724	0.000208	0.4557	- 80.522	- 80.843
Baghdad	Ka UL (30)	0.2251	0.3181	0.000401	0.5436	- 84.132	- 84.911
Amarah	Ku DL (12)	0.0169	0.0777	0.000127	0.0948	- 75.724	- 75.821
Amarah	Ku UL (14)	0.0270	0.0945	0.000148	0.1216	- 77.090	- 77.241
Amarah	Ka DL (20)	0.0684	0.3492	0.000247	0.4179	- 80.484	- 80.948
Amarah	Ka UL (30)	0.1885	0.3024	0.000478	0.4914	- 84.080	- 84.939

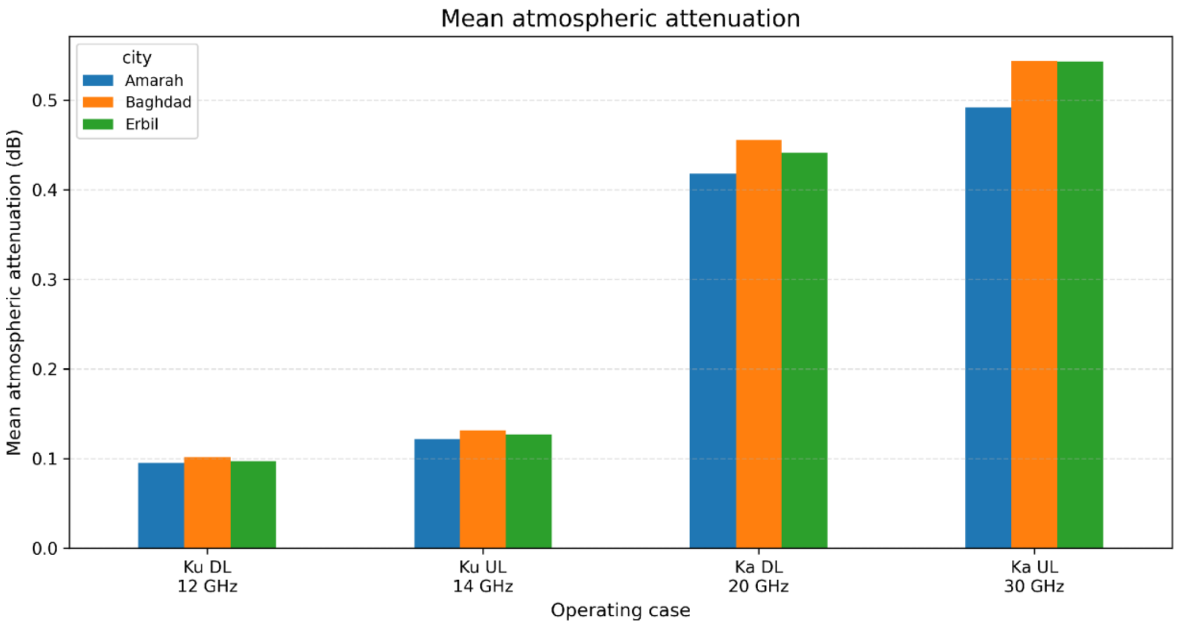

Fig. 6. Mean atmospheric attenuation for the four Ku/Ka operating cases.

The mean value of direct dust attenuation was very small (4.78×10^{-4} dB at 30 GHz for Amarah in the monthly calculation). The contribution of gas was around 55% of the mean loss in Erbil, 59% in Baghdad and 62% in Amarah at Ka uplink. Only slightly less, the loss was provided by rain. In all cities, the dust contribution is less than 0.1%.

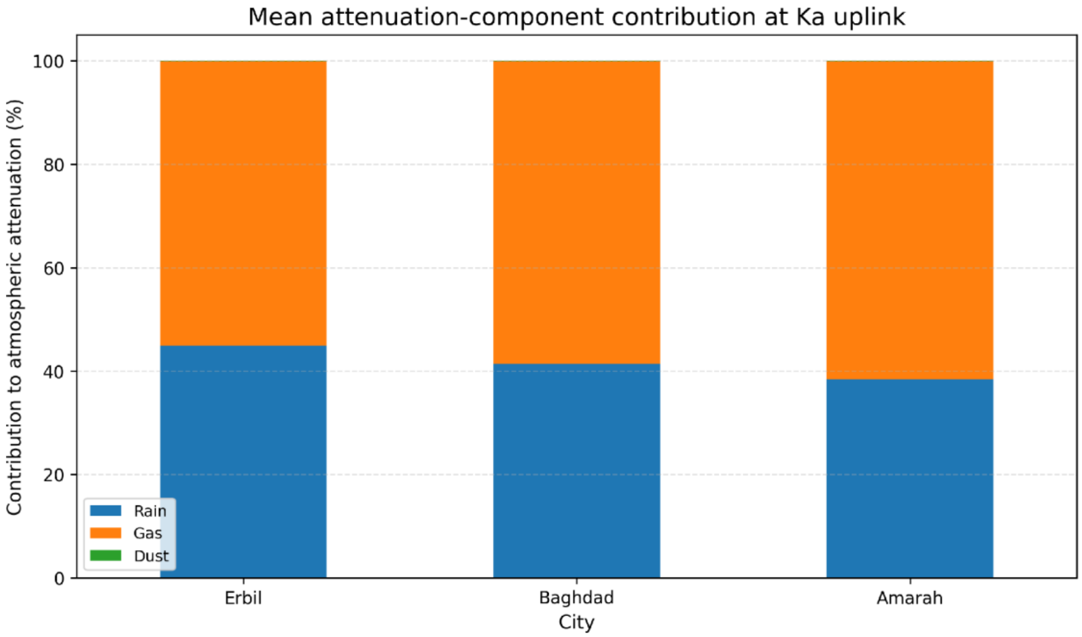

Fig. 7. Mean attenuation-component contributions at Ka uplink.

4.5 Received-power threshold sensitivity

Mean 30-GHz received power was -84.13 dBm in Erbil, -84.13 dBm in Baghdad, and -84.08 dBm in Amarah. The monthly minimas ranged from -84.91 to -84.94 dBm. As a result, values for each month were just above -85 and -87 dBm relative to the reference link, and values near -84.5 dBm were able to show significant differences between the months and cities.

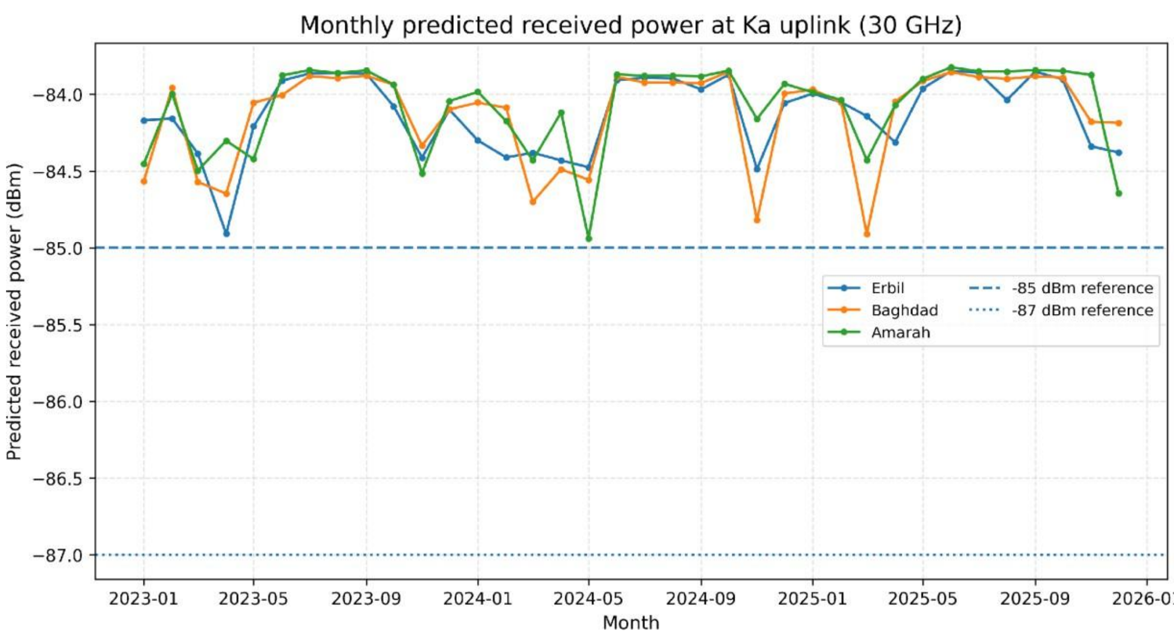

Fig. 8. Monthly predicted received power at Ka uplink.

Table 6. Ka-uplink threshold indicator for selected received-power levels.

Threshold (dBm)	Erbil	Baghdad	Amarah
-87.00	100.0%	100.0%	100.0%
-85.00	100.0%	100.0%	100.0%
-84.75	97.2%	94.4%	97.2%
-84.50	97.2%	80.6%	91.7%
-84.25	66.7%	75.0%	75.0%
-84.00	41.7%	50.0%	58.3%

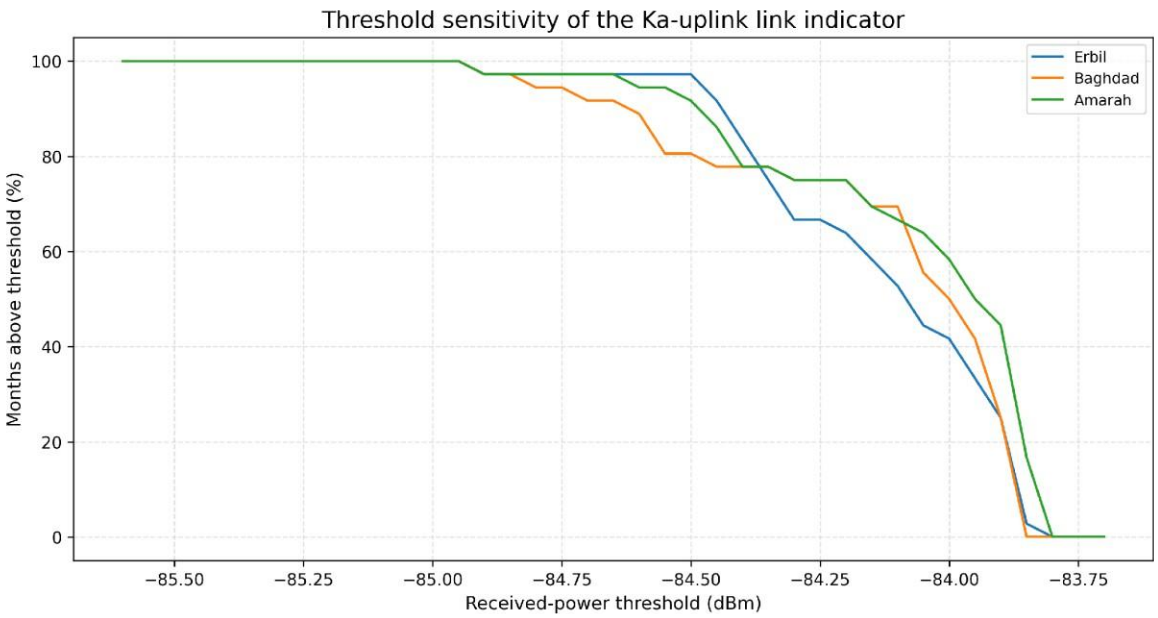

Fig. 9. Sensitivity of the Ka-uplink link indicator to the selected received-power threshold.

The curves illustrate why a certain percentage (threshold) should be associated with a receiver design. The change in T before month shifts, even with the same atmospheric model and with no changes to the environment, makes a significant difference in the percentage. The -87 dBm is a reference level, not a definition of satellite-link reliability in general.

4.6 Dust-concentration sensitivity

The peak monthly DUSMASS for each city was used along with the conservative bin coefficient to conduct a concentration-scaling analysis at 30 GHz. The dust attenuation due to the direct dust was less than 0.001 dB at the peak values observed. It took about 39 times as much as the Erbil peak to reach 0.01 dB, and 13.5 times as much as the Baghdad peak and 11.2 times as much as the Amarah peak. The values of the corresponding multipliers were two and three orders of magnitude greater for 0.1 and 1 dB.

Table 7. Multipliers of observed peak DUSMASS required for selected 30-GHz dust attenuation levels.

City	Peak DUSMASS	Peak Adust (dB)	× for 0.01 dB	× for 0.1 dB	× for 1 dB
Erbil	1.68e-07	0.000255	39.2	392.3	3923
Baghdad	4.89e-07	0.000740	13.5	135.2	1352

Amarah	5.91e-07	0.000894	11.2	111.9	1119

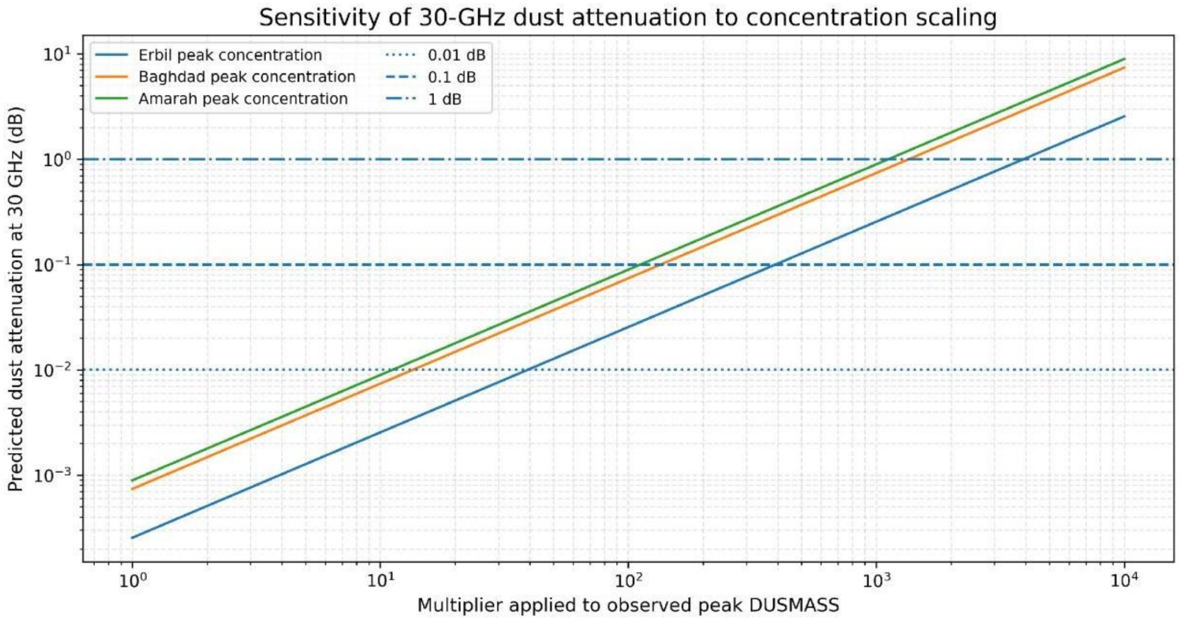

Fig. 10. Sensitivity of 30-GHz dust attenuation to concentration scaling.

This test will not simulate a specific storm. It determines the concentration scale suggested by the particle model and layer depth chosen. Losses could be different when short-lived plumes, larger particles, other mineralogy, non-spherical shapes or deeper vertical structures occur. Event-scale observations are required prior to the ability to interpret the multiplier as a storm probability.

5. Discussion

5.1 Regional environmental variability

The environmental inputs support an increase in the concentration of dust that is strong in the North-South direction, however the propagation outputs don't follow the concentration solely. The gaseous attenuation is dependent upon pressure, temperature and water vapour; the rain is dependent on the wettest-day input and the dust is dependent on concentration and mass extinction coefficient. The final rank of the respective cities is, therefore, slightly variable. This is a more realistic way of doing things than to dictate one impairment to be the dominant one for each region and season.

5.2 Relative importance of the atmospheric components

The largest atmospheric term at Ka band for the inputs used in this month is gaseous absorption. But even though the rain is smaller, it is still material, especially at 30 GHz. There's also direct dust extinction, which is much lower than both. The result is to be interpreted at the level of the input data, here the monthly means of the surface dust concentration and a uniform dust layer of 3 km. It does not demonstrate that intense Iraqi dust storms are able to affect all microwave links. It demonstrates that there is not enough field in the monthly DUSMASS to sustain a large direct fade in conjunction with the aforementioned small particle model.

5.3 Interpretation of MERRA-2 dust data

MERRA-2 is useful in that it is able to provide a consistent regional aerosol record, but each variable has a defined physical meaning. DUSMASS is not an optical depth, column mass or measured slant-path concentration. The bulk monthly product also does not contain the DU001-DU005 fractions that are needed to find an exact mixture coefficient. Reporting the bounded coefficient is then more defensible than assuming the unreported fractions. This component of the model would greatly benefit from event-scale bin-resolved mass mixing ratios, as well as vertical profiles.

5.4 Meaning of the reliability indicator

The threshold indicator converts the predicted power into a more comprehensible percentage; however, it is still a simulation indicator. The characteristics of a real receiver would be given as bandwidth, noise temperature, required E_b/N_0, modulation and coding, implementation loss, interference, and outage duration. With the current reference link, -85 and -87 dBm are below all the monthly 30GHz values and hence result in 100%. If the threshold is lowered nearer to -84.5 dBm, variability in the environment is seen. This sensitivity is valuable for design exploration purposes, but should not be reported as measured service availability.

5.5 Engineering implications

The model recommends three possible areas for initial Ku/Ka planning in Iraq. First, gaseous attenuation should be determined in relation to the state of the atmosphere and not by a constant, which is a frequency. Secondly, for rain studies the most possible fine time resolution available should be used and the full P.618/P.837 procedure adopted if the aim is to achieve availability. Third, before giving a large fade margin, you should also relate the presence of dust to the properties of the particles and to the vertical structure. Event-scale bin-resolved observations and synchronized beacon measurements would add more value for model validation, but more years of monthly DUSMASS would benefit the climatology.

6. Conclusions

A documented propagation model was built for Ku- and Ka-band satellite communication over Erbil, Baghdad and Amarah. The model is based on NASA POWER meteorology; MERRA-2 dust surface mass concentration; ITU-R free-space, rain and gaseous procedures; Rayleigh dust-extinction formulation and a generalized GEO link budget. The mean values of the attenuation of atmosphere were kept below 0.55 dB in all four operating cases. The largest monthly mean contribution was from gaseous absorption, followed by rain and direct dust attenuation was still less than 0.001dB for the available DUSMASS and path assumptions. There was a distinct trend in dust-loading throughout the region, but the concentration alone was not sufficient to predict the expected Ku/Ka loss. In all three cities mean received power was approximately the same at 30 GHz, and as illustrated in threshold analysis, the percentage-based reliability was very sensitive for the method used for receiver reference. The real benefit of the framework lies in its ability to de-couple the data, physical conversion, link assumptions, and interpretation. It can be used for comparative planning or for future validation studies, and event-scale particle information, vertical profiles of particle data, specific satellite geometry and synchronized link measurements will still be needed for operational prediction.

Data Availability

The NASA POWER Data Access Viewer and API make NASA POWER meteorological data freely accessible to the public. MERRA-2 M2TMNXAER aerosol diagnostics data are available at NASA GES DISC and Giovanni with dataset DOI 10.5067/FH9A0MLJPC7N. The monthly inputs and result tables are provided in the Supplementary Material.

Code Availability

The Supplementary Material includes pre-processed input tables, ITU-R P.676 spectroscopic tables (parsed), model results, and Python code to check the equations or to reproduce the output.

Author Contributions

Taghreed A. Noori: conceptualization, data curation, methodology, software, formal analysis, visualization, and writing - original draft. Hasanain A. H. Al-Behadili: supervision, validation, methodology review, project administration, and writing - review and editing.

Funding

The authors have no funding or financial/other interests to disclose.

Conflict of Interest

The authors declare no conflict of interest.

Acknowledgements

The authors are grateful to NASA POWER, NASA GMAO, and NASA GES DISC for their data services for meteorology and aerosol data that were utilized for this study.

References

1. T. Pratt, C. W. Bostian, and J. E. Allnutt, Satellite Communications, 2nd ed. Hoboken, NJ, USA: Wiley, 2003.
2. ITU-R, “Propagation data and prediction methods required for the design of Earth-space telecommunication systems,” Recommendation ITU-R P.618-14, International Telecommunication Union, Geneva, Switzerland, Aug. 2023.
3. ITU-R, “Calculation of free-space attenuation,” Recommendation ITU-R P.525-5, International Telecommunication Union, Geneva, Switzerland, Nov. 2024.
4. ITU-R, “Specific attenuation model for rain for use in prediction methods,” Recommendation ITU-R P.838-3, International Telecommunication Union, Geneva, Switzerland, Mar. 2005.
5. ITU-R, “Attenuation by atmospheric gases and related effects,” Recommendation ITU-R P.676-13, International Telecommunication Union, Geneva, Switzerland, Aug. 2022.
6. NASA POWER Project, “POWER Data Access Viewer and parameter documentation,” NASA Langley Research Center, accessed Jul. 2026.
7. NASA Global Modeling and Assimilation Office and S. Pawson, “MERRA-2 tavgM_2d_aer_Nx: 2d, monthly mean, time-averaged, single-level, assimilation, aerosol diagnostics V5.12.4,” NASA GES DISC, 2015, doi: 10.5067/FH9A0MLJPC7N.
8. R. Gelaro et al., “The Modern-Era Retrospective Analysis for Research and Applications, Version 2 (MERRA-2),” Journal of Climate, vol. 30, no. 14, pp. 5419-5454, 2017, doi: 10.1175/JCLI-D-16-0758.1.
9. C. A. Randles et al., “The MERRA-2 aerosol reanalysis, 1980 onward. Part I: System description and data assimilation evaluation,” Journal of Climate, vol. 30, no. 17, pp. 6823-6850, 2017, doi: 10.1175/JCLI-D-16-0609.1.
10. S. W. Berrick, G. Leptoukh, J. D. Farley, and H. Rui, “Giovanni: A web service workflow-based data visualization and analysis system,” IEEE Transactions on Geoscience and Remote Sensing, vol. 47, no. 1, pp. 106-113, 2009, doi: 10.1109/TGRS.2008.2003183.
11. A. B. Collow et al., Supplemental Documentation for GEOS Aerosol Products. NASA Global Modeling and Assimilation Office, 2023.
12. S. M. Sharif, “Attenuation properties of dusty media using Mie scattering solution,” Progress In Electromagnetics Research M, vol. 43, pp. 9-18, 2015, doi: 10.2528/PIERM15022403.
13. A. Musa, S. O. Bashir, and A. H. Abdalla, “Review and assessment of electromagnetic wave propagation in sand and dust storms at microwave and millimeter wave bands - Part I,” Progress In Electromagnetics Research M, vol. 40, pp. 91-100, 2014, doi: 10.2528/PIERM14102904.
14. A. Musa, S. O. Bashir, and A. H. Abdalla, “Review and assessment of electromagnetic wave propagation in sand and dust storms at microwave and millimeter wave bands - Part II,” Progress In Electromagnetics Research M, vol. 40, pp. 101-110, 2014, doi: 10.2528/PIERM14102903.
15. E. Alozie, A. Musa, N. Faruk, A. L. Imoize, et al., “A review of dust-induced electromagnetic waves scattering theories and models for 5G and beyond wireless communication systems,” Scientific African, vol. 21, e01816, 2023, doi: 10.1016/j.sciaf.2023.e01816.
16. S. A. A. Abdulla, H. M. Al-Rizzo, and M. M. Cyril, “Particle-size distribution of Iraqi sand and dust storms and their influence on microwave communication systems,” IEEE Transactions on Antennas and Propagation, vol. 36, no. 1, pp. 114-126, 1988, doi: 10.1109/8.1082.
17. A. A. Attiya and B. G. Jones, “Climatology of Iraqi dust events during 1980-2015,” SN Applied Sciences, vol. 2, 845, 2020, doi: 10.1007/s42452-020-2669-4.
18. S. A. Khidher, “Dust storms in Iraq: Past and present,” Theoretical and Applied Climatology, vol. 155, pp. 4721-4735, 2024, doi: 10.1007/s00704-024-04886-x.
19. S. M. Awadh, “Impact of North African sand and dust storms on the Middle East using Iraq as an example: Causes, sources, and mitigation,” Atmosphere, vol. 14, no. 1, 180, 2023, doi: 10.3390/atmos14010180.
20. S. Shrestha and D.-Y. Choi, “Study of rain attenuation in Ka band for satellite communication in South Korea,” Journal of Atmospheric and Solar-Terrestrial Physics, vol. 148, pp. 53-63, 2016, doi: 10.1016/j.jastp.2016.08.008.
21. K. C. Igwe, O. D. Oyedum, M. O. Ajewole, and A. M. Aibinu, “Evaluation of some rain attenuation prediction models for satellite communication at Ku and Ka bands,” Journal of Atmospheric and Solar-Terrestrial Physics, vol. 188, pp. 52-61, 2019, doi: 10.1016/j.jastp.2019.03.005.
22. D. Bolton, “The computation of equivalent potential temperature,” Monthly Weather Review, vol. 108, no. 7, pp. 1046-1053, 1980, doi: 10.1175/1520-0493(1980)108<1046:TCOEPT>2.0.CO;2.
23. ITU-R, “Characteristics of precipitation for propagation modelling,” Recommendation ITU-R P.837-8, International Telecommunication Union, Geneva, Switzerland, Sep. 2025.
24. A. H. Labban and M. J. Butt, “Evaluation of MERRA-2 data for aerosol patterns over the Kingdom of Saudi Arabia,” Heliyon, vol. 9, no. 6, e17047, 2023, doi: 10.1016/j.heliyon.2023.e17047.